RESEARCH ARTICLE

Macromolecular Chemistry and Physics
www.mcp-journal.de

Influence of Tacticity on the Structure Formation of Poly(methacrylic acid) in Langmuir/Langmuir–Blodgett and Thin Films

*Nazmul Hasan, Thi Minh Hai Nguyen, Karsten Busse, and Jörg Kressler**

A perfect isotactic poly(methacrylic acid) (*it*-PMAA) is synthesized and characterized by NMR spectroscopy. Surface pressure versus mean area per repeat unit (π–*A*) isotherms are recorded and compared with atactic poly(methacrylic acid) (*at*-PMAA). *it*-PMAA exhibits a π–*A* isotherm, indicating the formation of a stable Langmuir film. The isotherm has a characteristic pseudo-plateau at π of ≈11–14 mN m^{-1} attributed to the creation of worm-like entities confirmed by atomic force microscopy (AFM) in Langmuir–Blodgett (LB) films. These structures transform into spherical nanoparticles of ≈40 to 80 nm seen in LB films transferred at the end of the pseudo-plateau of the isotherm. Grazing incidence wide-angle X-ray scattering (GI-WAXS) shows a broad scattering signal (halo-like) at a *q* position of ≈11.12 nm^{-1}, revealing the amorphous nature of the nanoparticles. An ordered morphology, however, is observed in thin films prepared by precipitating *it*-PMAA from dimethylformamide (DMF) solution under vigorous stirring and coating them on a solid support. Optical microscopy (OM), AFM, and GI-WAXS reveal more details about the structure. Finally, various structural modifications of PMAAs are explained based on their tacticity and the subsequent hydrogen bonding effects between the carboxylic acid groups.

1. Introduction

Tacticity in polymers refers to the configurational arrangement of pendant/side groups with respect to the polymer backbone. The three main arrangements are isotactic (*it*), syndiotactic (*st*), and atactic (*at*). An isotactic polymer consists only of meso diads (*m*), for example, two adjacent configurational repeating units with identical orientation, whereas a syndiotactic polymer is made up of only racemo diads (*r*), that is, two adjacent configurational repeating units with the opposite orientation. An atactic polymer contains both *m* and *r* diads in a random sequence (**Scheme 1**).[1,2] Tacticity can be further described even more precisely with the introduction of higher-order sequences than diads such as triads (isotactic *mm*, syndiotactic *rr*), tetrads, and pentads. Another configuration is therefore possible referred to as the heterotactic (*mr*) triad. The fraction of higher-order sequences (e.g., triad) can be measured quantitatively by NMR spectroscopy.[3,4] Tacticity is very important since it influences various polymer properties as solubility, crystallization, and mechanical properties.[1] Iso- and syndiotactic polymers are often semi-crystalline, whereas atactic polymers are amorphous as observed in many flexible chain polymers like poly(propylene).[1,5,6] The scenario is different for acrylic polymers such as poly(methyl methacrylate) (PMMA)[7] or poly(acrylic acid) (PAA).[8,9] Even iso- or syndio-tactic rich configurations are still amorphous. Different approaches including solvent/acid treatment,[8–11] high-temperature annealing,[7] stretching,[7] or even compression, for example, in Langmuir films[12,13] were applied to crystallize them. The latter approach provides less entanglements and more mobility to the polymer chains, which facilitates increased crystallization rates. Upon compression on the water surface of a Langmuir trough *it*-PMMA crystallizes in a matter of hours[13,14] while other techniques generally take weeks.[15,16] It also allows crystallizing polymers in monolayers that help to reveal molecular-level information as, for example, double helices by atomic force microscopy (AFM) in Langmuir–Blodgett (LB) films.[13,17,18] Poly(methacrylic acid) (PMAA) is another acrylic polymer that can be prepared with varying tacticities or stereoregular forms (e.g., *it*-, *at*-, and *st*-PMAA).[19] Tacticity significantly affects the solubility, conformational transitions, and structure formation of PMAAs. For instance, *it*-PMAA is a water-insoluble polymer compared to other stereoisomers.[20] The pH-induced conformational transition of compact coil to an extended structure in *it*-PMAA is irreversible,[21] whereas it is reversible in *at*-PMAA.[22,23] The conformation of *it*-PMAA in solution is helical as compared

N. Hasan, T. M. H. Nguyen, K. Busse, J. Kressler
Department of Chemistry
Martin Luther University Halle-Wittenberg
D-06120 Halle/Saale, Germany
E-mail: joerg.kressler@chemie.uni-halle.de

The ORCID identification number(s) for the author(s) of this article can be found under https://doi.org/10.1002/macp.202200428

DOI: 10.1002/macp.202200428

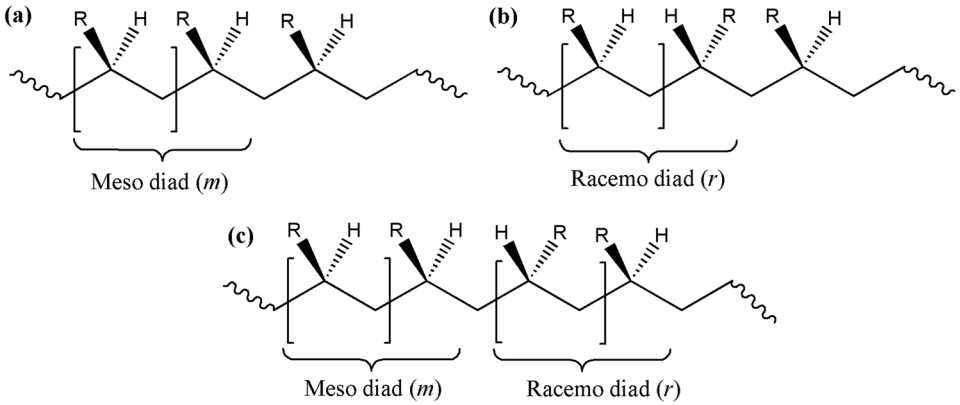

Scheme 1. Zigzag projection of a) isotactic, b) syndiotactic, and c) atactic configuration of a polymer. The bracket shows one configurational repeating unit. The *R* is the pendant/side group with respect to the hydrocarbon backbone.

to the curve-like structure of *st*-PMAA.[24] The temperature has also a strong influence on the structure formation of PMAAs in aqueous solutions.[25] A thermo-reversible gelation was found in *it*-PMAA at low temperatures, but for *at*-PMAA in concentrated solutions at high temperatures.[20,25] Crystalline-like precipitates were reported for *it*-PMAA in dimethylformamide (DMF) solution when stirred for a week.[26] So far, the structure formation of *it*-PMAA is strongly dependent on the degree of neutralization of the acid groups.[20,26] The formation of intra- and intermolecular hydrogen bonds between the acid groups and van der Waals forces between α-methyl units of the polymer are responsible for various structures in PMAA stereoisomers.[20,23,26] In the majority of the studies, the tacticity effect was evaluated by comparing *it*-PMAA with *at*-PMAA[23] and rarely with *st*-PMAA.[24,27] This is because polymers considered as *at*-PMAA have in fact an excess of syndiotactic units.[28] Thus, the structure formation of *st*-PMAA (which in fact does not exist with high purity) was therefore found to be similar to *at*-PMAA.[24] In contrast to the structures formed in solution, all stereoisomers of PMAA are predominantly amorphous in the solid state, even for PMAA containing ≈92% to 97% isotactic triads.[20,26] Different approaches were employed for the structure formation of PMAAs in bulk or thin films. For example, *it*-PMAA thin films prepared from DMF solution and then treated with water are believed to yield crystalline polymer with helix formation.[20] In some studies, Langmuir films of *it*-PMAA[29] and LB films of *at*-PMAA[30] were prepared. However, there were no detailed reports concerning the film morphology, chain ordering, and orientation of *it*-PMAA Langmuir/LB and thin films. Also, PMAA used in most of the thin film studies had a low isotactic content (e.g., 92% isotactic triads).[20]

Here, we synthesized a poly(methacrylic acid) (PMAA) containing isotactic triads (*mm*) of more than 99% which can be considered as a perfect *it*-PMAA. The structure formation in thin films fabricated by the Langmuir/LB and suspension-cast methods was investigated and compared with *at*-PMAA. Langmuir films were prepared at the air-water interface. Langmuir–Blodgett (LB) films were prepared by transferring Langmuir films to solid supports. Furthermore, stirring induced structures of *it*-PMAA in DMF solution were coated on solid supports to prepare thin films considered here as suspension-cast films. Finally, the morphology and chain ordering (e.g., crystallization) of the films are studied by optical microscopy (OM), AFM, and GI-WAXS techniques.

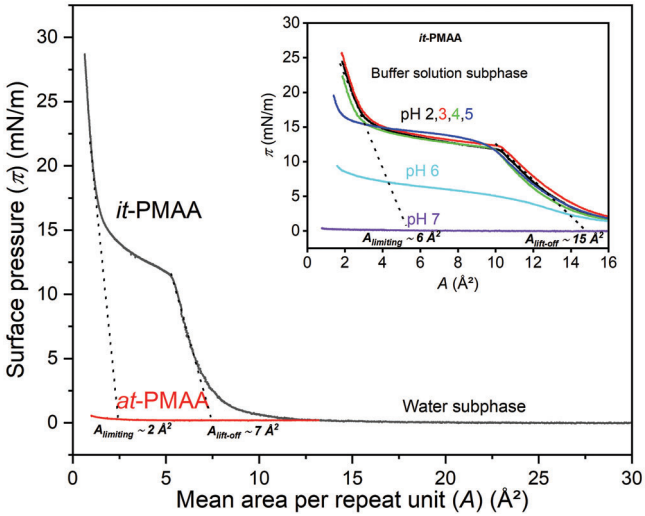

Figure 1. π–A isotherm of *it*- and *at*- PMAA recorded at 20 °C on the water surface. The insert represents the isotherms of *it*-PMAA measured with aqueous subphases of different pH values. The dotted lines are added to indicate the lift-off ($A_{\text{lift-off}}$) and limiting (A_{limiting}) area values. The isotherm also exhibits a hysteresis as shown in Figure S1, Supporting Information along with the elastic modulus plot.

2. Result and Discussion

2.1. π–A isotherms, Langmuir, and LB films of PMAA

The π–A isotherms depicted in **Figure 1** were measured to confirm the Langmuir film formation of two different PMAAs. The isotherms were recorded by dissolving the polymers in a suitable solvent (e.g., dimethyl sulfoxide (DMSO) for *it*-PMAA and water for *at*-PMAA), spreading the polymer solutions on the water surface of a Langmuir trough, and then compressing the adsorbed polymer molecules by moving the barriers of the trough. *it*-PMAA exhibits π–A isotherms, which primarily indicate the

formation of a stable Langmuir film. The shape of the isotherm looks quite similar to the previously reported isotherm of *it*-PMAA with less isotactic content.[29] The lift-off ($A_{\text{lift-off}}$) and limiting (A_{limiting}) area per repeat unit, however, were found slightly smaller in the present study. It should be noted that extremely small limiting areas in $\pi-A$ isotherms are an indication of flakes or multilayer films or aggregation formation rather than the Langmuir monolayer films.[31,32] Now, we will carefully analyze the isotherm, particularly the area values in order to learn more about the film formation.

As can be seen in *it*-PMAA Langmuir isotherm that π increases monotonically at an $A_{\text{lift-off}}$ of ≈7 Å^2 followed by a plateau-like zone at ≈ 11–14 mN m^{-1} and reaches to a maximum π of ≈ 28 mN m^{-1} upon decreasing A. The limiting area (A_{limiting}) per repeat unit is estimated as ≈2 Å^2 by drawing a tangent at the end of the isotherm to $\pi = 0$ mN m^{-1}. The repeat unit area of *it*-PMAA should be ≈23.1 Å^2 calculated considering a rectangular box (≈5.5 × 4.2 Å) (Figure S2, Supporting Information). Limiting areas of some similar polymers estimated from the Langmuir isotherm were *it*-PMMA ≈23–26 Å^2[33] and poly(methyl acrylate) (PMA) ≈23 Å^2.[34] The observed area value of *it*-PMAA is therefore notably too small for being a monolayer, implying that some molecules enter the subphase during spreading of the polymer from DMSO solution and film compression, retaining a small fraction of the polymer molecules on the water surface. This is possible since the spreading solvent DMSO is water-miscible. Another reason for observing a small A value would also be the solubilization effect caused by the ionization/deprotonation of carboxylic acid groups of the polymer. The latter statement was verified by changing pH values from 2 to 7 of the subphase. This time, π increases at an A of ≈15 Å^2 followed by slightly extended plateaus for the subphase pH of 2 to 5 (Figure 1 inset). Now, a slightly larger limiting area of ≈6 Å^2 is found. Interestingly, a drastic change in the isotherm is observed at subphase pH values of 6 to 7. A more extended isotherm with a plateau (7–9 mN m^{-1}) at a subphase pH of 6 can be identified. The change of the isotherm shape upon changing pH suggests some conformation transition (coil to extended structure) of *it*-PMAA molecules due to the acid group ionization.[35] As can be seen in Figure 1, no isotherm is possible at a subphase pH of 7, meaning that the Langmuir film of *it*-PMAA is only stable up to a certain subphase pH. This is because at a subphase pH of 7, more than 33% carboxylic groups of *it*-PMAA can be ionized as calculated by the Henderson-Hasselbalch equation[36] considering pK_a value of *it*-PMAA ≈7.3.[37,38] The ionization enhances the hydrophilicity of the polymer chain and solubilizes the Langmuir film in the water subphase. In bulk, *it*-PMAA becomes water soluble when more than 20% of acid groups are ionized/deprotonated.[20] So, it is obvious that even in a low pH subphase condition (nonionized condition), the lift-off and limiting areas are still small (i.e., 6, 15 Å^2). To obtain morphological information, Brewster angle microscopy (BAM) and epifluorescence imaging of the Langmuir film of *it*-PMAA have been employed. No film morphology was observed by both of the microscopies (BAM images in Figure S3, Supporting Information). This indicates that the structure of *it*-PMAA Langmuir films is significantly smaller than that of many other Langmuir polymer films (LPF).[14,39,40] Some bright spots can be seen in epifluorescence images, suggesting microparticle formation incorporated with dye molecules (**Figure 2**b,c). At high surface compression, the number of bright spots (microparticles) increases as well as some dark lines appear (Figure 2d). The dark contrast is the denser parts of the Langmuir film with fewer or no dye molecules. This is very different from the commonly seen dark contrast in epifluorescence images of Langmuir polymer films that happened due to the dye molecules exclusion caused by crystallization.[41,42]

In short, solubility and microparticle formation are the two main reasons for small limiting area values in the $\pi-A$ isotherm of *it*-PMAA. Since the Langmuir isotherm is based on the assumption that all molecules stay on the water subphase and adsorb, therefore, dissolution or loss of the molecules makes the area calculation inaccurate. Another point is that the pH of the pure water subphase is ≈5.7 due to the reaction with atmospheric CO_2.[43] The value can be further reduced to below 4.7 due to the surface propensity of hydronium ions.[43] As a result, carboxylic acid ionization/deprotonation is extremely low, allowing stable Langmuir films to be formed also on the pure water subphase. In contrast to the *it*-PMAA Langmuir isotherm, the *at*-PMAA shows no increase of π upon decreasing A, meaning no Langmuir film formation. This happens due to the water-soluble nature of the polymer as well as the spreading solvent effect. Langmuir films of some water-soluble polymers such as poly(ethylene oxide) (PEO)[44] and poly(vinyl alcohol) (PVA)[45] were also reported. Typically, chloroform is used as the spreading solvent for PEO and the observed Langmuir film is stable up to a π of ≈8 mN m^{-1}.[46] It can be reached to ≈38 mN m^{-1} using a subphase of concentrated aqueous salt solution.[44] The PVA is however spread from the water solution and π can be reached to ≈17 mN m^{-1}.[45] Now, it is evident that tactility strongly affects the Langmuir film formation of different stereoisomers of PMAA. Further characterizations of the Langmuir films were done by transferring the films to the solid supports referred to as LB films. **Figure 3** shows AFM images of LB film made before the pseudo-plateau region of the isotherm at π of ≈7 mN m^{-1}. Some tiny entities (bright spots) with an average dimension of ≈30 nm and thickness of ≈2.3 nm can be observed. These are some nanoaggregates of *it*-PMAA formed during the film transfer process or already in the Langmuir film. The amount of these entities is significantly small, therefore, the whole substrate surface is fairly empty. This also suggests that the *it*-PMAA Langmuir film before the plateau pressure is in the liquid phase and has no transferable structure.

The scenario is completely different for the LB films transferred at the plateau region of the isotherm. Two different structures were identified as microparticles and nanostructures. The microparticles with dimensions ranging from ≈1 to 10 μm can be seen by optical microscopy (Figure S4, Supporting Information). Scanning electron microscopy (SEM) analysis revealed that the particles have a highly porous structure (not shown here). AFM imaging was solely done in the areas of the LB film where these microparticles were not present (thickness ≥4 μm, not suitable for AFM). **Figure 4a** shows AFM images of the LB film made at π of ≈12 mN m^{-1}. Randomly distributed worm-like nanostructures with an average thickness of ≈2 nm can be observed. The substrate surface is now almost covered by these worms. A high-resolution AFM cantilever was also used to analyze the surface

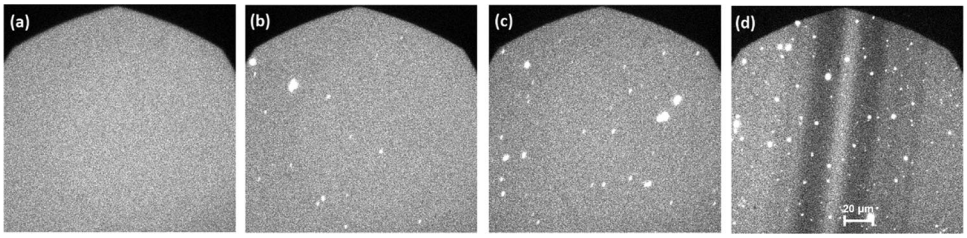

Figure 2. Epifluorescence image of a) aqueous Rhodamine-B dye subphase and b–d) *it*-PMAA Langmuir film on the aqueous Rhodamine-B dye subphase at different π values such as ≈2, ≈12, and ≈17 mN m^{-1}.

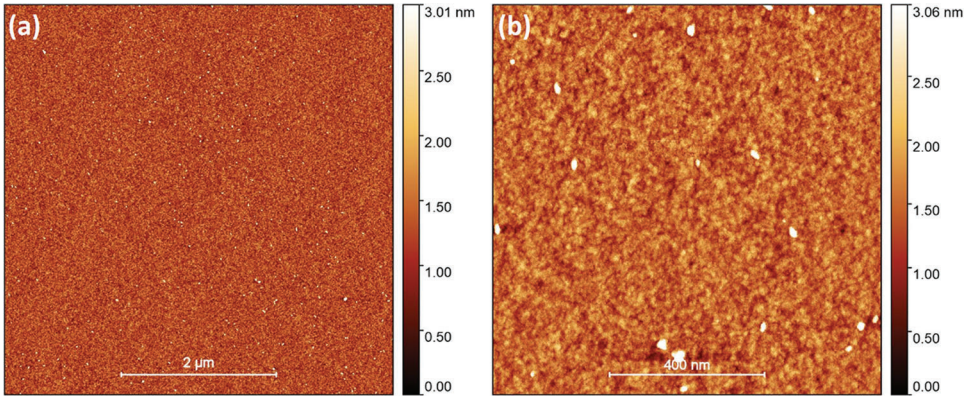

Figure 3. AFM height image of *it*-PMAA LB film recorded with different scan sizes a) 5 × 5 µm and b) 1 × 1 µm. The film was transferred before the plateau region of the isotherm at a π of ≈7 mN m^{-1}.

of the worms, however, other than their smooth surface, no further information can be explored. This may happen due to the limitations of the AFM instrument or because the structures are located inside of the nanoaggregates similar to *it*-PMAA diblock copolymer.[47] Figure 4b is an AFM image of the LB film made at the end of the plateau of the isotherm ($\pi \approx 17$ mN m^{-1}). Many spherical nanoparticles with the dimension of ≈40 to 80 nm can be seen. Now the substrate is completely covered by the nanoparticles. The average roughness of the film is estimated as ≈4.5 nm, suggesting some sort of multilayer formation. It is also obvious that side-by-side associations of them appeared like a pearl chain structure. In conclusion, LB films of *it*-PMAA possess worm-like structures at the plateau pressure of the π–A isotherm and are then transformed into spherical nanoparticles at high surface compression after ≈15 mN m^{-1}.

Typically, aggregates or micelles are observed in Langmuir films of completely hydrophobic polymers like poly(styrene)[31] or diblock copolymers containing hydrophobic blocks.[48] Langmuir films of amphiphilic polymers often show flat films or crystallites,[14,41,49] which is clearly not the case in *it*-PMAA.

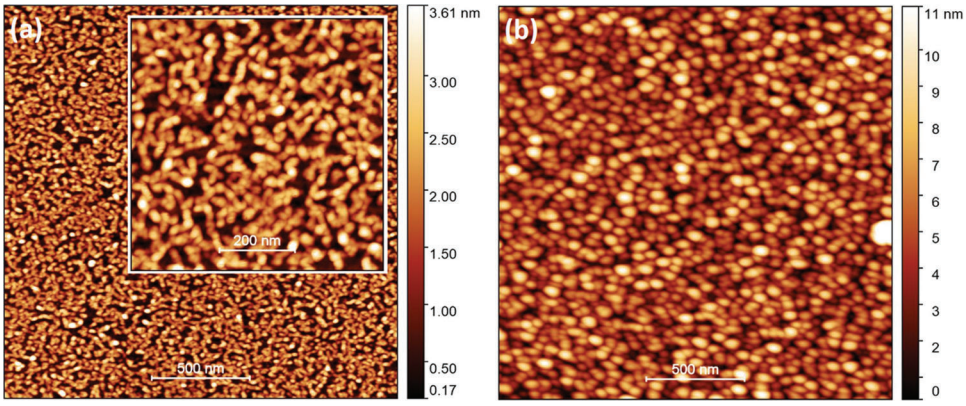

Figure 4. AFM height image of *it*-PMAA LB film transferred at π of a) ≈12 mN m^{-1} and b) ≈17 mN m^{-1} of the π–A isotherm. The inset in the left image is a magnified view. The height distribution of both images is given in Figure S5, Supporting Information. Besides, in Figure S6, Supporting Information, AFM images with large scan areas of the LB film are presented.

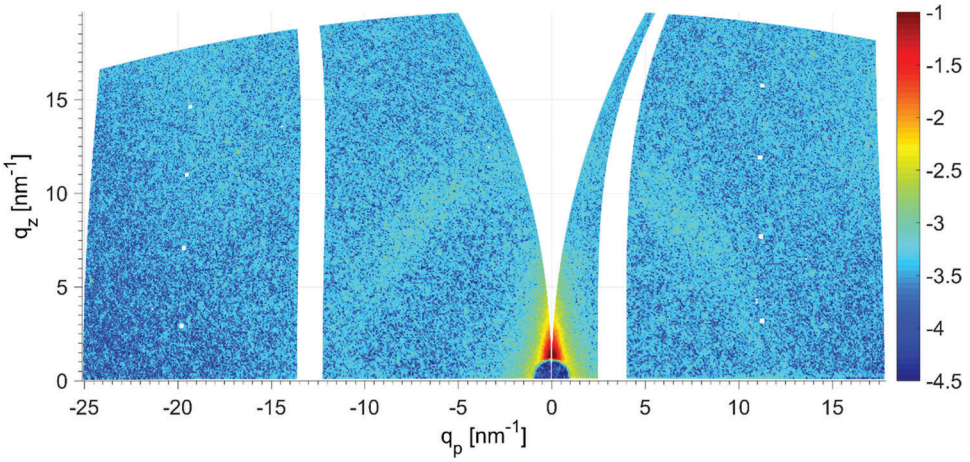

Figure 5. 2D GI-WAXS image of *it*-PMAA LB film transferred by vertical dipping at ≈17 mN m^{-1} on a silicon substrate. The logarithmic color scale was adjusted to visualize the less-intense signal.

After spreading the polymer solution, the acid groups of *it*-PMAA anchor to the water surface, and the hydrophobic methyl groups stay in the air. The *it*-PMAA films at the oil/water interface also showed similar behavior, for example, aggregation-free extended chain conformation.[38] We also observed no significant aggregates (except some microparticle formation) in Langmuir/LB films made before the plateau zone of the isotherm. This confirms that the polymer molecules were well adsorbed on the water surface without film collapse. However, during compression, *it*-PMAA chains come very close to each other (at the plateau region), which facilitates intra- or inter-molecular hydrogen bonding among the acid groups and exposes the methyl groups to the water surface. This process immediately promotes aggregation (nanoparticle formation) since the methyl groups do not like the water surface. Continuing the film compression, some aggregates combined with each other to form a worm-like shape, and finally, transformed into spherical nanoaggregates after the plateau zone of the isotherm (Figure 4b). LB films transferred even afterward have similar structures with higher film thickness, suggesting multilayer formation. From the above findings, we can state that the plateau zone in the isotherm is appearing due to a transition from the liquid film phase to worm-like aggregates followed by nanoparticle formation. Additionally, the structures of the Langmuir film might also be altered slightly during the film-transferring (vertical dipping) and drying processes. GI-WAXS studies were finally done in order to reveal the chain ordering (crystallization) of nanoparticles. **Figure 5** shows a GI-WAXS image of *it*-PMAA LB film transferred at the end of the plateau zone ($\pi \approx 17$ mN m^{-1}). A weak broad arc-like scattering signal at a q value of ≈11.12 nm^{-1} corresponding to d of ≈0.56 nm was identified. A similar scattering signal at $2\theta \approx 15.6°$ ($d = 0.56$ nm) along with some other signals at $2\theta \approx 23°$ and ≈ 32° was observed in wide-angle X-ray scattering (WAXS) measurements of the powder/granular sample of *it*- and *at*- PMAA (Figure S7, Supporting Information). All these scattering signals are related to some short-range average intra- and inter- chain distances of *it*-PMAA assigned to amorphous halos.[26,50] Thus, the Langmuir and subsequent LB films of *it*-PMAA may also be amorphous. Interestingly, the arc-like scattering signal in the GI-WAXS image has a high-intensity distribution (anisotropy) at 45° with respect to the surface normal, suggesting some kind of preferred orientation present in *it*-PMAA chains. It should be noted that a diblock copolymer of *it*-PMAA crystallized with nanosphere or nanofiber formation when precipitated by water from the DMSO solution.[47] Similar types of nanospheres were also found in the present studies, however, they are completely amorphous as confirmed by GI-WAXS. Furthermore, crystallization of *it*-PMAA with helix formation was sometimes achieved in thin films by water treatment.[20] Therefore, all LB films were further treated with water for more than 15 days. However, no new reflection appeared in the GI-WAXS experiments. It is obvious that *it*-PMAA LB films are predominantly amorphous and does not crystallize by any treatment. We believe that Langmuir film formation of *it*-PMAA by compression promotes strong hydrogen bonding among the acid groups of the polymer chains and van der Waals forces among the methyl groups. This causes fast aggregation and prevent the crystallization process. The hydrogen bonding sometimes promotes or prevents crystallization in many systems including Langmuir films of small molecules.[51] It is also important to point out that GI-WAXS was not successful for the LB films transferred at the plateau region of the isotherm (≈12 mN m^{-1}) due to the presence of fewer polymer material.

2.2. Structure Formation of *it*-PMAA in Thin Films

In contrast to the LB films, another type of thin film was prepared by precipitating *it*-PMAA from DMF solution with vigorous stirring at room temperature. The precipitates were collected and coated on glass slides/silicon substrates to make thin films. We immediately checked the films by optical and polarized optical microscopy (POM). Some petal- or needle-like structures can be identified (**Figure 6**), which also show strong birefringence under POM, suggesting anisotropic behavior as commonly seen in polymer crystallization.[52] These petals or needles are randomly oriented in the film with different dimensions ranging from ≈50 to 200 μm. They could be crystallites of *it*-PMAA based on their

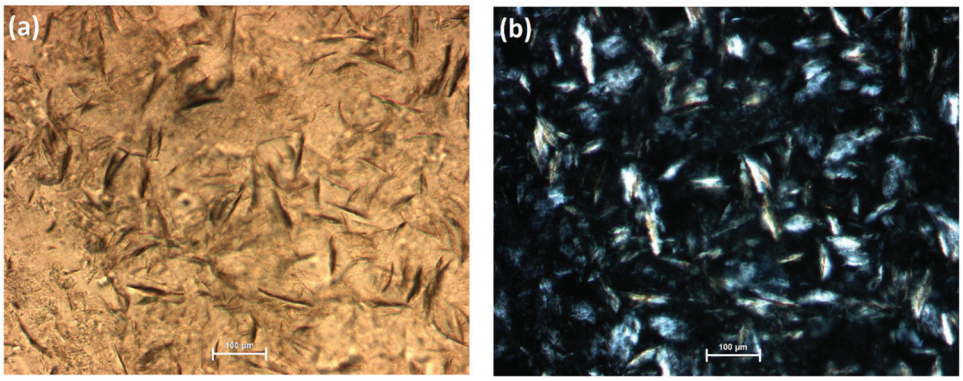

Figure 6. a) Optical microscopy image of *it*-PMAA thin films prepared by precipitating the polymer from DMF solution and b) polarized optical microscopy image of the same film.

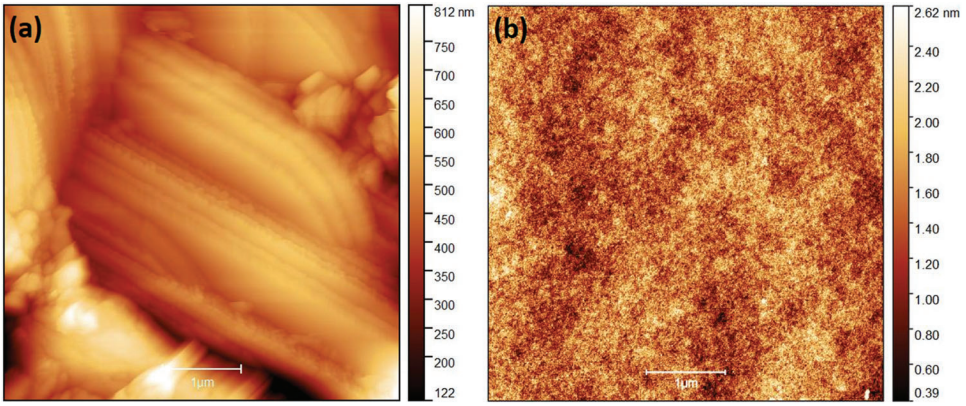

Figure 7. AFM height image of a) *it*-PMAA thin films containing petals/needles and b) *at*-PMAA thin films prepared by the solution-cast method.

appearance under 20× magnification (Figure S8, Supporting Information).

AFM was utilized in order to gain a deeper understanding on the morphology of the petals/needles. **Figure 7a** is an AFM height image recorded on one of the petals or needles present on the *it*-PMAA thin film. A fiber/layered-like structure can be identified compared to *at*-PMAA films, which possess no structure in Figure 7b (smooth film). A gel-like morphology was observed in some places of the films (Figure S9, Supporting Information). So, it is hard to conclude about the general morphology of these petals or needles. Sometimes the fibers are covered by amorphous *it*-PMAA particles. Besides, the *it*-PMAA thin film is quite rough (>1 µm), which generates artifacts and makes the imaging difficult.

So, GI-WAXS was used for further characterization of the films concerning crystallization and chain orientations. **Figure 8** shows a GI-WAXS image of *it*-PMAA thin films containing these petals/needles. A new broad Bragg reflection at a q_z value of ≈12.9 nm^{-1} corresponds to a d value of ≈0.49 nm can be identified. The scattering intensity is significantly distributed at the q_z axis, which confirms that the *it*-PMAA chains in the petals have a preferred orientation, for example, chains are parallel to the substrate surface. A similar Bragg reflection ($2\theta \approx 18.1°$) was reported for *it*-PMAA thin film containing ≈90% isotactic triads prepared by precipitating the polymer from DMF solution with vigorous stirring.[26] It should be noted that a similar polymer such as *it*-PAA crystallizes with fiber formation in protonated/nonionized conditions.[8] Since *it*-PMAA is also in a same condition (non-neutralized in DMF solution), crystallization with fiber formation may happen. Typically, electrostatic repulsion forces among the ionized acid groups hinder the chain packing necessary for crystallization.[8,9] The reason for ordered structures can be explained by hydrogen bond formation. The *it*-PMAA is internally well-ordered, therefore, hydrogen bonding among the acid groups can occur in a more cooperative way. This is not possible in case of *at*-PMAA due to the tacticity effect, for example, randomly distributed acid groups in the structure.[23] Additionally, methacrylic acid crystalizes with dimer formation under high pressure and low-temperature conditions due to the hydrogen bonding effect.[53]

3. Conclusion

The structure formation of two different stereoisomers such as isotactic (*it*)- and atactic (*at*)- PMAA in thin films prepared by Langmuir/LB and suspension-cast methods was investigated. The formation of Langmuir/LB film is strongly tacticity and subphase pH dependent. The *it*-PMAA can form stable Langmuir films below a subphase pH value of 7 as confirmed by $\pi-A$ isotherm measurements as a function of subphase pH. The

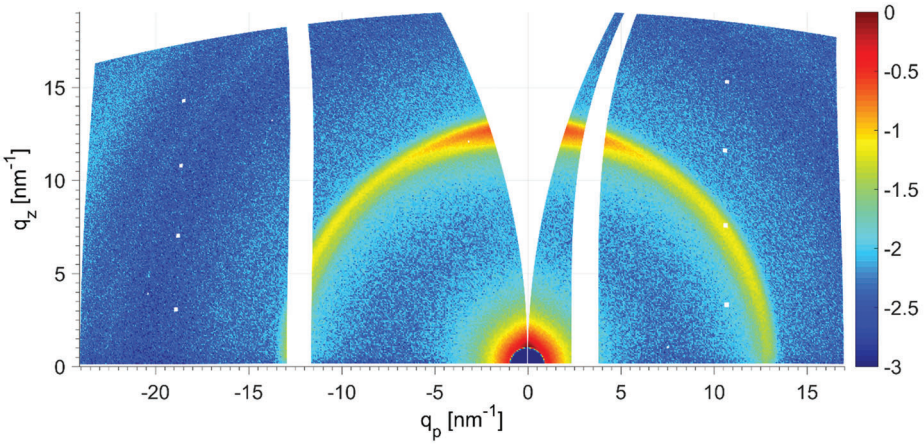

Figure 8. 2D GI-WAXS image of *it*-PMAA thin films prepared by precipitating the polymer from the DMF solution, coating them on a silicon substrate, and drying. The logarithmic color scale was adjusted to visualize the less-intense signal.

film possesses a worm-like structure at the plateau region of the $\pi-A$ isotherm followed by the formation of nanoparticles at high surface compression after the plateau region. These nanoaggregates are amorphous as revealed by the GI-WAXS technique. Hydrogen bonding and van der Waals forces are the two main forces that cause these structures. The *at*-PMAA on the other hand cannot form Langmuir and subsequent LB films due to the water-soluble nature of the polymer. Besides, thin films prepared by precipitating *it*-PMAA from DMF solution under mechanical stirring, coating the precipitates on the solid support, and drying show characteristic ordered structures (petals/needles) in OM/POM as compared to *at*-PMAA. AFM imaging exhibits fiber or layered structures in the petals or needles. Finally, GI-WAXS confirmed that these structures are well ordered, suggesting some sort of crystallites of *it*-PMAA.

4. Experimental Section

Materials: The two stereoisomers of PMAA under investigation are *it*- and *at*- PMAA. *it*-PMAA with an isotactic triad (*mm*) of ≥99% and a molar mass of 17 200 g mol^{-1} was synthesized using reversible addition-fragmentation chain-transfer (RAFT) polymerization.[54] The synthesis details can be found in the supporting document of Figures S10–S13, Supporting Information. PMAA (AB127082) with a molar mass of 20 000 g mol^{-1} was purchased from abcr GmbH (Germany). The tacticity% of the sample is (*it*:*ht*:*st* = 10:35:55) determined by ^{1}H NMR spectroscopy and considered here as *at*-PMAA (supporting information Figure S14, Supporting Information).[3] The buffer solutions with pH ranging from 2 to 7, HPLC grade DMSO, and DMF were purchased from Carl Roth GmbH (Germany). Rhodamine B fluorescence dye (83 689) was bought from Sigma Aldrich GmbH (Germany).

$\pi-A$ Isotherms, Langmuir/LB Film Preparation: A Langmuir trough from Riegler & Kirstein Germany with an area of 545 cm^2 was used to record $\pi-A$ isotherms for both PMAAs. The trough contains two symmetrical moveable barriers and a Wilhelmy plate system to measure surface pressure (π). Millipore water and different buffer solutions with pH from 2 to 7 were used as subphases for the experiments. The subphase was kept at 20 °C using a thermostat and the whole trough was covered by a Plexiglas box to maintain stable conditions. The purity of the subphase was checked prior to the isotherm measurements by surface pressure measurement at maximum barrier compression ($\pi < 0.15$ mN m^{-1}). Polymer solutions with a concentration of ≈2 mg mL^{-1} were prepared in DMSO for *it*-PMAA and water for *at*-PMAA since none of the polymers are soluble in chloroform. The isotherms were recorded by spreading the polymer solution dropwise in some random location on the subphase using a Hamilton digital syringe, then compressing the trough surface at a speed of 50 Å^2 per molecule min^{-1}). The $\pi-A$ isotherms were well reproducible under the above-mentioned experimental conditions with some marginal variation in the mean area per repeat unit values. This happened because *it*-PMAA losses into the water subphase due to the spreading solvent effect, for example, spreading more polymer solution causes more polymer loss which results in slightly smaller area values. The shape of the isotherms however was found to be consistent. A similar situation was reported for the Langmuir isotherm of PAA-based diblock copolymers.[55]

LB films were prepared at various transfer pressures such as ≈7, ≈12, and ≈17 mN m^{-1}. Several silicon substrates with a size of 20 × 10 mm^2 were rinsed with ethanol, dipped in sulfuric acid for 30 min, and then washed with distilled water. The substrates were then extensively cleaned using a CO_2 snow jet and hooked immediately vertically to the transfer unit of the instrument in order to prevent contamination of the substrates. The substrate was then immersed into the subphase of ≈8 mm before the monolayer formation. The polymer solutions were then spread on the water surface and compressed up to the transfer pressure. When the transfer pressure was reached, the submerged silicon substrate was moved upward at a speed of ≈0.5 mm min^{-1} while maintaining π constant. This process transferred the Langmuir films on both sides of the substrate surface. The films were then left to dry at room temperature and stored in a sealed box for AFM and GI-WAXS measurements.

Epifluorescence Microscopy: Axio Scope A1 Vario microscope from Carl Zeiss Microimaging Germany coupled with a Riegler & Kirstein Langmuir trough was used for epifluorescence imaging of *it*-PMAA Langmuir film. The images were acquired with an EC Epiplan-NEOFLUAR 50× objective and a Hamamatsu EM-CCD digital camera. An aqueous solution of Rhodamine B fluorescence dye with a concentration of 50 nM was used as a subphase. The temperature of the subphase was kept at 20 °C. The dye was excited using a mercury arc lamp through a combination of BP 546/12 nm window and a beam splitter FT 560 nm. The emission was detected via a BP 575–640 nm (filterset 20, Carl Zeiss, Germany). The imaging of the Langmuir films was performed during film compression at a speed of 50 Å^2 per molecule min^{-1}).

Thin Film Preparation: 5 mg solid powder of *it*-PMAA was dissolved in 5 mL HPCL grade DMF solution under stirring using a magnetic stirrer at room temperature. The solution was continued stirring vigorously until some white-colored particles (turbidity) were seen. These particles were collected by 5 min centrifugation at 6000 rpm and coated on a glass slide for optical or polarized optical microscopy analysis and on the silicon substrate for AFM, and GI-WAXS studies.

Polarized Optical Microscopy: Axioplan 2 polarized microscope from Carl Zeiss Germany was used to conduct the optical and polarized optical microscopy studies. All images were recorded in transmission mode at magnifications between 10× to 20× using an Axio Cam MRc camera.

Atomic Force Microscopy: MultiMode 8 instrument from Bruker USA was used to perform AFM studies on the *it*-PMAA LB films. Peak-Force Quantitative Nanomechanics (PF-QNM) tapping mode with a SCANSYST-AIR cantilever (spring constant of 0.4 N m^{-1} and resonance frequency of 70 kHz) was used for the measurements. The images were recorded with a cantilever oscillation of 2 kHz, a scan speed of 0.5 Hz, and a number of lines of 512. The captured images were then processed by Gwyddion software.

Grazing Incidence Wide-Angle X-Ray Scattering: Retro-F SAXSLAB setup from Copenhagen Denmark was used for GI-WAXS measurements. The instrument was equipped with an AXO microfocus X-ray source (Dresden, Germany) and a DECTRIS PILATUS3 R 300K detectors (Baden-Daettwil, Switzerland). Measurements were performed in the reflection mode at room temperature under vacuum conditions. The incidence angle α_i was $\approx 0.2^{\circ}$ near the silicon critical angle $\alpha_c = 0.22^{\circ}$ for Cu$K\alpha$ radiation ($\lambda = 1.5418$ Å). The obtained detector image was converted to the reciprocal coordinates according to the literature.[56,57]

Supporting Information

Supporting Information is available from the Wiley Online Library or from the author.

Acknowledgements

N.H. and T.M.H.N. are both first authors and contributed to this work equally. This work was supported by Deutsche Forschungsgemeinschaft (Project B07 of SFB TRR 102, project number 189853844). AFM and GI-WAXS measurements were supported by Prof. Thomas Thurn-Albrecht within the SFB TRR 102. The authors also acknowledge Dr. Oleksandr Dolynchuk for the conversion of GI-WAXS images.

Open access funding enabled and organized by Projekt DEAL.

Conflict of Interest

The authors declare no conflict of interest.

Data Availability Statement

The data that support the findings of this study are available from the corresponding author upon reasonable request.

Keywords

atomic force microscopy, grazing incidence wide-angle X-ray scattering, isotactic poly(methacrylic acid), Langmuir–Blodgett and thin films

Received: November 29, 2022
Revised: December 22, 2022
Published online: January 18, 2023

[1] E. M. Woo, L. Chang, in *Encyclopedia of Polymer Science and Technology*, Wiley, Hoboken, NJ **2011**.
[2] C. M. Fellows, K.-H. Hellwich, S. V. Meille, G. Moad, T. Nakano, M. Vert, *Pure Appl. Chem.* **2020**, *92*, 1769.
[3] A. J. White, F. E. Filisko, *J. Polym. Sci., Polym. Lett. Ed.* **1982**, *20*, 525.
[4] T. Uryu, T. Asakura, K. Matsuzaki, *NMR Spectroscopy and Stereoregularity of Polymers*, Karger Publishers, Basel **1996**.
[5] R. P. Quirk, *J. Chem. Educ.* **1981**, *58*, 540.
[6] G. Natta, P. Corradini, *Nuovo Cim.* **1960**, *15*, 40.
[7] A. De Boer, G. O. R. A. Van Ekenstein, G. Challa, *Polymer* **1975**, *16*, 930.
[8] V. A. Kargin, S. Y.a. Mirlina, V. A. Kabanov, G. A. Mikheleva, *Polym. Sci. U.S.S.R.* **1962**, *3*, 34.
[9] V. A. Kargin, V. A. Kabanov, S. Y.a. Mirlina, A. V. Vlasov, *Polym. Sci. U.S.S.R.* **1962**, *3*, 28.
[10] T. G. Fox, B. S. Garrett, W. E. Goode, S. Gratch, J. F. Kincaid, A. Spell, J. D. Stroupe, *J. Am. Chem. Soc.* **1958**, *80*, 1768.
[11] J. Spevácek, B. Schneider, J. Baldrian, J. Dybal, J. Stokr, *Polym. Bull.* **1983**, *9*, 495.
[12] R. H. G. Brinkhuis, A. J. Schouten, *Macromolecules* **1991**, *24*, 1487.
[13] J. Kumaki, T. Kawauchi, E. Yashima, *J. Am. Chem. Soc.* **2005**, *127*, 5788.
[14] C. Fuchs, K. Busse, A. -K. Flieger, J. Kressler, *Chem. Eng. Technol.* **2016**, *39*, 1333.
[15] K. Buyse, H. Berghmans, *Polymer* **2000**, *41*, 1045.
[16] H. Kusanagi, H. Tadokoro, Y. Chatani, *Macromolecules* **1976**, *9*, 531.
[17] J. Kumaki, T. Kawauchi, K. Okoshi, H. Kusanagi, E. Yashima, *Angew. Chem., Int. Ed.* **2007**, *46*, 5348.
[18] Y. Ono, J. Kumaki, *Macromolecules* **2018**, *51*, 7629.
[19] K. Hatada, *J. Polym. Sci., Part A: Polym. Chem.* **1999**, *37*, 245.
[20] E. Van Den Bosch, Q. Keil, G. Filipcsei, H. Berghmans, H. Reynaers, *Macromolecules* **2004**, *37*, 9673.
[21] J. C. Leyte, H. M. R. Arbouw-Van Der Veen, L. H. Zuiderweg, *J. Phys. Chem.* **1972**, *76*, 2559.
[22] B. Jerman, K. Kogej, *Acta Chim. Slov.* **2006**, *53*, 264.
[23] S. Sitar, V. Aseyev, K. Kogej, *Soft Matter* **2014**, *10*, 7712.
[24] C. Podlipnik, K. Kogej, *Acta. Chim. Slov.* **2007**, *54*, 509.
[25] P. Hribersek, K. Kogej, *Macromolecules* **2019**, *52*, 7028.
[26] E. Van Den Bosch, H. Berghmans, *Polym. Bull.* **2007**, *58*, 153.
[27] N. A. Valley, E. J. Robertson, G. L. Richmond, *Langmuir* **2014**, *30*, 14226.
[28] V. Crescenzi, in *Fortschritte Der Hochpolym*, Springer-Verlag, Berlin, Heidelberg, **1968**, pp. 358–386.
[29] R. H. G. Brinkhuis, A. J. Schouten, *Langmuir* **1992**, *8*, 2247.
[30] C. Mengel, A. R. Esker, W. H. Meyer, G. Wegner, *Langmuir* **2002**, *18*, 6365.
[31] J. Kumaki, *Macromolecules* **1988**, *21*, 749.
[32] W.-P. Hsu, Y.-L. Lee, S.-H. Liou, *Appl. Surf. Sci.* **2006**, *252*, 4312.
[33] J. Miñones, M. M. Conde, E. Yebra-Pimentel, J. M. Trillo, *J. Phys. Chem. C* **2009**, *113*, 17455.
[34] J. M. Hammond, M. H. Williams, W. G. P. Robertson, *Nature* **1961**, *189*, 549.
[35] L. Ruiz-Pérez, A. Pryke, M. Sommer, G. Battaglia, I. Soutar, L. Swanson, M. Geoghegan, *Macromolecules* **2008**, *41*, 2203.
[36] T. Swift, *Acrylate Polymers for Advanced Applications*, IntechOpen, London **2020**.
[37] H. Dong, H. Du, X. Qian, *J. Phys. Chem. B* **2009**, *113*, 12857.
[38] D. K. Beaman, E. J. Robertson, G. L. Richmond, *Proc. Natl. Acad. Sci. U. S. A.* **2012**, *109*, 3226.
[39] N. Hasan, C. Fuchs, C. Schwieger, K. Busse, O. Dolynchuk, J. Kressler, *Polymer* **2020**, *196*, 122468.
[40] N. Hasan, K. Busse, A. Ullah, H. Hussain, J. Kressler, *Langmuir* **2021**, *37*, 13399.
[41] N. Hasan, K. Busse, T. Haider, F. R. Wurm, J. Kressler, *Polymers* **2020**, *12*, 2408.
[42] N. Hasan, C. Schwieger, H. T. Tee, F. R. Wurm, K. Busse, J. Kressler, *Eur. Polym. J.* **2018**, *101*, 350.
[43] V. Buch, A. Milet, R. Vácha, P. Jungwirth, J. P. Devlin, *Proc. Natl. Acad. Sci. U. S. A.* **2007**, *104*, 7342.

[44] C. Fuchs, H. Hussain, E. Amado, K. Busse, J. Kressler, *Macromol. Rapid Commun.* **2015**, *36*, 211.
[45] F. Boury, T. Z. Ivanova, I. Panaiotov, J. E. Proust, A. Bois, J. Richou, *J. Colloid Interface Sci.* **1995**, *169*, 380.
[46] N. Hasan, A. Ullah, S. Ullah, J. Kressler, H. Hussain, *Colloid Polym. Sci.* **2019**, *297*, 1149.
[47] H. Ajiro, M. Akashi, *Macromol. Rapid Commun.* **2010**, *31*, 714.
[48] J. Zhu, R. B. Lennox, A. Eisenberg, *J. Phys. Chem.* **1992**, *96*, 4727.
[49] K. Busse, C. Fuchs, N. Hasan, M. Pulst, J. Kressler, *Langmuir* **2018**, *34*, 12759.
[50] A. J. Christofferson, G. Yiapanis, J. M. Ren, G. G. Qiao, K. Satoh, M. Kamigaito, I. Yarovsky, *Chem. Sci.* **2015**, *6*, 1370.
[51] C. Li, P. Hilgeroth, N. Hasan, D. Ströhl, J. Kressler, W. H. Binder, *Int. J. Mol. Sci.* **2021**, *22*, 12679.
[52] U. W. Gedde, *Polymer Physics*, Chapman & Hall, London **1995**.
[53] I. D. H. Oswald, A. J. Urquhart, *CrystEngComm* **2011**, *13*, 4503.
[54] K. Ishitake, K. Satoh, M. Kamigaito, Y. Okamoto, *Macromolecules* **2011**, *44*, 9108.
[55] Z. Guennouni, M. Goldmann, M.-C. Fauré, P. Fontaine, P. Perrin, D. Limagne, F. Cousin, *Langmuir* **2017**, *33*, 12525.
[56] O. Dolynchuk, P. Schmode, M. Fischer, M. Thelakkat, T. Thurn-Albrecht, *Macromolecules* **2021**, *54*, 5429.
[57] K. Busse, C. Fuchs, N. Hasan, M. Pulst, J. Kressler, *Langmuir* **2018**, *34*, 12759.